Easy access to energy fluctuations in non-equilibrium quantum many-body systems

Marcela Herrera,[1, 2, *] John P. S. Peterson,[3] Roberto M. Serra,[2, †] and Irene D'Amico[4, ‡]

[1]*Departamento de Ciencias Naturales, Universidad Autónoma de Occidente, Cali, Colombia*
[2]*Centro de Ciências Naturais e Humanas, Universidade Federal do ABC,*
Avenida dos Estados 5001, 09210-580 Santo André, São Paulo, Brazil
[3]*Institute for Quantum Computing and Department of Physics and Astronomy,*
University of Waterloo, Waterloo N2L 3G1, Ontario, Canada
[4]*Department of Physics, University of York, York YO10 5DD, United Kingdom*

We combine theoretical and experimental efforts to propose a method for studying energy fluctuations, in particular, to obtain the related bi-stochastic matrix of transition probabilities by means of simple measurements at the end of a protocol that drives a many-body quantum system out-of-equilibrium. This scheme is integrated with numerical optimizations in order to ensure a proper analysis of the experimental data, leading to physical probabilities. The method is experimentally evaluated employing a two interacting spin-1/2 system in a nuclear magnetic resonance setup. We show how to recover the transition probabilities using only local measures which enables an experimental verification of the detailed fluctuation theorem in a many-body system driven out-of-equilibrium.

Energy fluctuations play a significant role on the out-of-equilibrium thermodynamics of quantum systems [1–3]. They are inherently related to fluctuation relations [4–11], which embraces both thermal and quantum energy fluctuations. In this context thermal fluctuations are, generally, related with thermal distributions at the beginning of a driving protocol or at the end of a thermalization process, while quantum fluctuations are associated to transitions between eigenstates in a quantum dynamics, depending on how the systems is driven. Here, work and heat are described by stochastic variables with probability distributions [1–3, 11]. The experimental verification or use of quantum fluctuation relations requires the assessment of both types of energy fluctuations [12].

Here we introduce a powerful method to experimentally access energy fluctuations of a many-body system in an out-of-equilibrium quantum evolution. More specifically we show how to reconstruct the bi-stochastic matrix of transition probabilities $p_{m|n}$ between the initial and final eigenstates of a driven protocol that determines quantum fluctuations. We then use the matrix to reconstruct the quantum work probability distribution. It can also be used to reconstruct the statistics of other quantities such as heat in the absence of work. Previous methods for this purpose are very demanding when applied to many-body systems since they involve controlled operations, as the interferometric method proposed in [13, 14]. In fact, so far, they have been employed in NMR experiments with one-body (i.e. two level) quantum systems, such as in Refs. [15–18] or in the quantum work meter implemented on an ensemble of non-interacting two-level atomic systems [19]. An efficient protocol to experimentally investigate energy fluctuations in a general out-of-equilibrium many-body system remains an outstanding challenge: the aim of this letter is to provide a long stride towards this goal by introducing a fresh approach. Previously we developed methods inspired by density-functional-theory (DFT [20]) [21–23] to support numerical calculations of energy fluctuations for out-of-equilibrium many-body system, a tough problem in itself; here we focus on providing directly an experimental method for measuring these quantities.

The transition probabilities among instantaneous eigenstates $p_{m|n}$ allow us to access the statistical properties of a time-dependent driven system and it is intimately related to quantities in the out-of-equilibrium thermodynamics as the work and entropy production. The work is one of the key quantities to describe the change of energy when an external agent acts on the system. The work performed on a quantum system is not an observable, but instead, it is determined by the way the process is executed [24, 25]. For a protocol much faster than the typical interaction time scale with the environment [42] , the mean work performed on or by a quantum system can be written as $\langle W \rangle = \int P(W)dW$, where the work probability distribution is $P(W) = \sum_{n,m} p_n^0 p_{m|n} \delta \left(W - \epsilon_m^\tau + \epsilon_n^0 \right)$, with p_n^0 is the probability to find the system in the initial eigenstate $|n(0)\rangle$, the transition probability $p_{m|n} = |\langle m(\tau)|\mathcal{U}_\tau|n(0)\rangle|^2$ is the conditional probability of driving the system to the instantaneous eigenstate $|m(\tau)\rangle$ (with energy ϵ_m^τ) at the end of the evolution, given the initial state $|n(0)\rangle$ (with energy ϵ_n^0), where $\mathcal{U}_\tau$ is the time evolution operator. We note that the transition probability $p_{m|n}$ is the quantity that defines how the driving processes is performed and it is also a key element in the determination of the entropy production in the protocol [9, 16, 26].

Conventionally, we can obtain $p_{m|n}$ by means of the so-called two-point measurement protocol [7, 10, 24, 28]. In this protocol, the system is initially prepared in the thermal equilibrium state, then the eigenstates of the initial Hamiltonian $\mathcal{H}_0$ are measured, through a non-destructive measurement represented by the projectors $\Pi_n^0 = |n(0)\rangle\langle n(0)|$. After that, the system is evolved due

to the variation of a parameter of the Hamiltonian, whose evolution is described by the operator $\mathcal{U}_\tau$. Finally, the eigenstates of the final Hamiltonian $\mathcal{H}_\tau$ are measured and this measurement is represented by the projectors $\Pi_m^\tau = |m(\tau)\rangle\langle m(\tau)|$. Eventually, from the measurement of the full statistics, it is possible to obtain $p_{m|n}$. The extension of the two-point measurement protocol to open systems was proposed in [27]. Performing such non-destructive projective measurements with high accuracy in an experiment is a very difficult task, even in a few-body system. Other theoretical protocols include generalized energy measurements as Gaussian energy measurements [29] and positive operator valued measurements (POVM) [30]. Another possibility is to use an interferometric protocol as employed in Refs. [13–16, 18] that requires a good control of each part of the many-body system and of the interaction between its constituents, which is challenging to implement experimentally even in few-body systems. Here, we propose an alternative way to obtain the transition probabilities $p_{m|n}$ through the direct determination of a set of observables, *easy to measure* in a given context.

Inversion scheme. Our protocol relies on an inversion scheme to obtain $p_{m|n}$ and is based on similar ideas to those given in Ref. [31] in the context of DFT. Let us consider measuring the mean value of an operator $\mathcal{O}$ at the end of a time-dependent protocol described by the evolution operator $\mathcal{U}_\tau$ that drives the system. We assume that initially the system is prepared in a thermal state ρ_0^{eq}, for a given thermal energy $k_B T$, with an initial Hamiltonian $\mathcal{H}_0$. The system will evolve according to $\mathcal{U}_\tau$ and during this process all allowed transitions between energy levels may occur. At time τ, corresponding to the end of the evolution, the mean value of a suitable observable, $\langle\mathcal{O}\rangle$, is measured. We can decompose this in terms of the instantaneous Hamiltonian energy basis as $\langle\mathcal{O}(\tau)\rangle = \sum_{m,m',n} \mathcal{O}_{m,m'} p_n^0 T_{m,m'|n}$, where $\mathcal{O}_{m,m'}$ are the operator matrix elements written on the basis of the final Hamiltonian $\mathcal{H}_\tau$, p_n^0 is the initial Gibbs distribution, and $T_{m,m'|n} = \langle m(\tau)|\mathcal{U}_\tau|n(0)\rangle\langle n(0)|\mathcal{U}_\tau^\dagger|m'(\tau)\rangle$ represents the transition elements, with $p_{m|n} = T_{m,m|n}$. It is important to highlight that the transition elements are *independent* both from the initial temperature and from the choice of $\mathcal{O}$. Instead, they only depend on how ('fast' or 'slow') the evolution of the system is performed. Hence, we may choose an operator $\mathcal{O}$ which is diagonal in the basis of $\mathcal{H}_\tau$, or in other words $[O, \mathcal{H}_\tau] = 0$, thus $\langle\mathcal{O}(\tau)\rangle = \sum_{m,n} \mathcal{O}_m p_n^0 p_{m|n}$ and we recover the transition probability $p_{m|n}$ between the instantaneous eigenstates of the initial and final Hamiltonians[43].

The key idea of our method is to write a system of linear equations based on the mean value $\langle\mathcal{O}\rangle$, where the set of variables are given by the elements $p_{m|n}$. For a system of Hilbert space dimension d, we should find $d \times d$ different transition probabilities. However, the square matrix $p_{m|n}$ is a bi-stochastic matrix, implying that, for each m
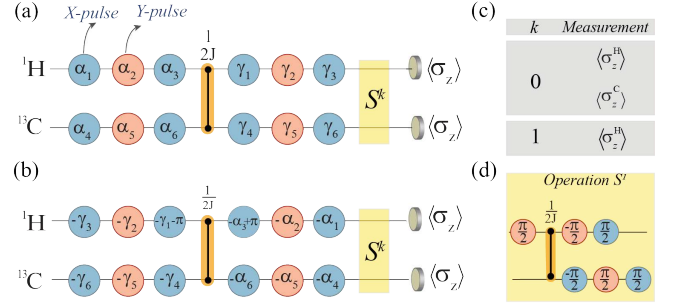

Figure 1. **Pulse sequence for the driven dynamics and measurement protocols.** In the sketch of the pulse sequence the blue (red) circles represent transverse rf pulses in the x (y) direction that produce rotations by the displayed angle. The orange connections represent free evolutions under the scalar interaction $\mathcal{H}_J = hJ\sigma_z^H\sigma_z^C/4$ (with $J \approx 215.1$ Hz) during the time $1/(2J)$. (a) Displays the sequence to implement the forward protocol. (b) Represents the sequence to implement the backward version of the driving protocol. (c) Indicates which local measures should be carried out depending on the value of k. (d) Represents the operation S^1 (S^0 is the identity). The values for α_i and γ_i are displayed in [32].

and n, the system is subject to the normalization conditions $\sum_m p_{m|n} = 1$ and $\sum_n p_{m|n} = 1$. Our system of linear equations can then be reduced to $(d-1) \times (d-1)$ elements. Thereby, if we have a two-level system, obtaining the corresponding four transition probabilities with the use of the normalization conditions intakes finding just one additional equation. For a system with a higher dimension we can find $(d-1) \times (d-1)$ equations by using different temperatures and/or measuring additional operators, so to construct a matrix equation of the form $\mathcal{A}\boldsymbol{x} = \boldsymbol{b}$ as [32]

$$\mathcal{A} = \begin{bmatrix} a_{11}^1 & a_{12}^1 & \cdots & a_{d',d'}^1 \\ a_{11}^2 & a_{12}^2 & \cdots & a_{d',d'}^2 \\ \vdots & \vdots & \ddots & \vdots \\ a_{11}^{d'\times d'} & a_{12}^{d'\times d'} & \cdots & a_{d',d'}^{d'\times d'} \end{bmatrix}, \boldsymbol{x} = \begin{bmatrix} p_{1|1} \\ p_{1|2} \\ \vdots \\ p_{d',d'} \end{bmatrix}, \boldsymbol{b} = \begin{bmatrix} b_1 \\ b_2 \\ \vdots \\ b_{d',d'} \end{bmatrix}$$
(1)

where $d' = d - 1$, $\boldsymbol{b}$ represents constants independent of $p_{m|n}$ and the superscript in the constant coefficients a_{mn}^j represents the different choices of operators and temperatures. Additionally, we can also use the symmetries of the system to further reduce the number of variables. To summarize, we aim to combine different observables and initial temperatures to get enough linear independent equations to allow reconstruction of the bi-stochastic matrix $p_{m|n}$. The number of observables needed depends on the symmetries of the initial and final Hamiltonians. As the measurements are done at the final time, they are independent from the energy difference across the transition. In the spirit of DFT, we aim to use as observable local magnetization or local particle densities. We present ideas for general applications of the method to large systems in the supplemental material[32].

Experimental implementation. In order to test our pro-

(a) **Forward protocol**
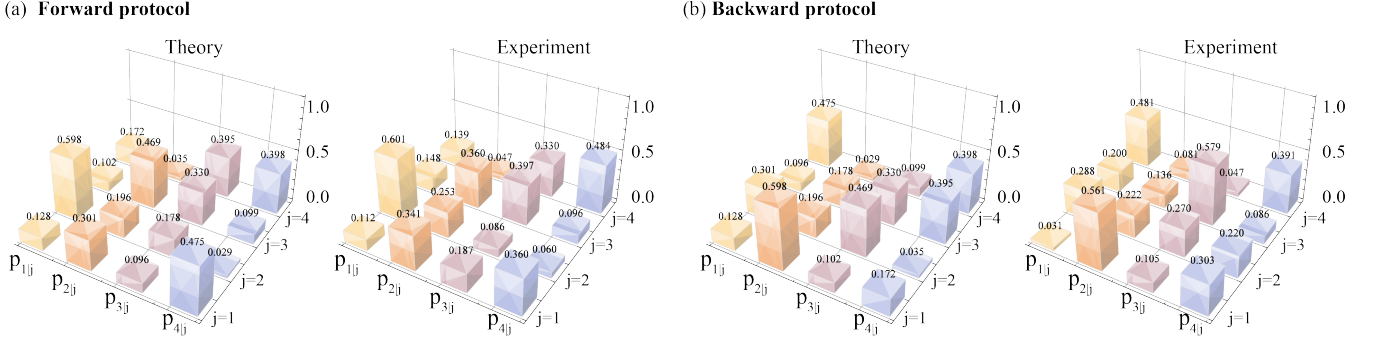

(b) **Backward protocol**

Figure 2. **Transition probabilities.** Transition probabilities obtained by the inversion scheme for the (a) forward and (b) backward protocols . For each protocol we show the comparison between the expected result given by the numerical simulation of the protocol (theory) and the experimental result. The elements $(p_{i|j})$ of the transition probability matrix are represented by the columns in the figure and their values are above the columns.

posed scheme for many-body systems let us consider an out-of-equilibrium evolution for a system of two interacting spins. This is significantly more complex than the single-qubit systems measured in some previous quantum thermodynamics experiments [15–18, 33, 34], as the number of transitions $p_{m|n}$ changes from 4 to 16. For the experiment, we employed a ^{13}C-labeled CHCl$_3$ liquid sample and a 500 MHz Varian NMR spectrometer. The relevant nuclear spin Hamiltonian for this molecule, in a rotating frame [32], is similar to the Ising model and can be written as [35]

$$\mathcal{H} = -\frac{1}{2}h\delta\nu_{\mathrm{H}}\sigma_z^{\mathrm{H}} - \frac{1}{2}h\delta\nu_{\mathrm{C}}\sigma_z^{\mathrm{C}} + \frac{1}{4}hJ\sigma_z^{\mathrm{H}}\sigma_z^{\mathrm{C}}, \qquad (2)$$

where $\delta\nu_H$ and $\delta\nu_C$ are the difference between the Larmor frequency and the rf-field frequency for the Hydrogen and the Carbon nuclei, respectively, and $J \approx 215.1$ Hz is the coupling constant. For this experiment we have chosen $\delta\nu_{\mathrm{H}} = 2.0$ kHz and $\delta\nu_{\mathrm{C}} = 4.0$ kHz. Time-modulated rf-field pulses in the transverse (x and y) direction combined with longitudinal field gradient pulses are used to prepare initially thermal states. The rf-field pulses can also be used to drive the nuclear spins provoking transitions between the eigenstates of the Hamiltonian.

For testing our method, we consider a general driven evolution of the two spins-1/2 system, which is implemented through a set of rf pulses and free evolutions. At the beginning and at the end of the evolution, the Hamiltonian of the system will be given by Eq. (2) defining the reference energy levels. As demonstrated in Ref. [36] a general two-qubit evolution can be realized by a circuit consisting of 12 elementary one-qubit gates and 2 CNOT gates. Since our goal is to perform a proof-of-principle experiment, we are not concerned in knowing what is the exact time-dependency in the Hamiltonian that implements such evolution. What we want, is to implement an evolution that produces as many as possible non-zero transition probabilities between the initial and

final energy eigenstates, in order to produce a non-trivial work probability distribution. To this aim, we can consider just a subclass of the general evolutions proposed in Ref. [36]. To test the detailed quantum fluctuation relation [8], we implement forward ($\mathcal{U}_F$) and backwards ($\mathcal{U}_B$) evolutions, by applying the unitary operations depicted in the pulse sequences of Fig. 1, (a) and (b), respectively. For $\mathcal{U}_B$ to be the time reversal evolution of $\mathcal{U}_F$, we have to apply all the pulses in the inverse order starting with the angles γ_i and finishing with the angles α_i. Also, $\gamma_i \to -\gamma_i$ and $\alpha_i \to -\alpha_i$ to satisfy $\mathcal{U}_B = \mathcal{U}_F^\dagger$. Finally, by an appropriate choice of the angles α_i and γ_i we can obtain an out-of-equilibrium evolution that produces several transitions between the initial and final eigenstates.

Since we are dealing with a system of dimension 4 (two spin 1/2), there will be a total 16 transition probabilities that describe the work distribution in the driving protocol. By using the bi-stochastic properties of the transition matrix $p_{m|n}$, our problem reduces to find 9 transitions probabilities only. Hence, in order to construct the system of equations (1), we can measure three observables – chosen to be the longitudinal magnetizations σ_z^{H}, σ_z^{C}, and the correlation function $\sigma_z^{\mathrm{H}}\sigma_z^{\mathrm{C}}$ – at three different effective spin temperatures, $k_B T_1 = 20 \pm 3$ peV, $k_B T_2 = 12 \pm 2$ peV, and $k_B T_3 = 9 \pm 2$ peV (for more details related to the initial thermal states see [32]). These chosen observables commute with the Hamiltonian (2), which simplify the numerical analysis in the inversion scheme. To obtain $\langle \sigma_z^{\mathrm{H}} \rangle$ and $\langle \sigma_z^{\mathrm{C}} \rangle$ in the NMR experiment, we apply a $\pi/2$ rotation in the y-direction and measure the traverse magnetization, which is the natural observable in NMR ($k = 0$ in Fig. 1). For obtaining the correlation function $\langle \sigma_z^{\mathrm{H}}\sigma_z^{\mathrm{C}} \rangle$, we consider $k = 1$, with the operation S^1 being just a CNOT gate written in terms of the rf pulses. Then at the end of the protocol we have to measure the magnetization in the z-direction of the Hydrogen $\langle \sigma_z^H \rangle$, as indicated in the grey table of Fig. 1(c). Therefore, at the end of the day, we are measuring the local magnetizations for obtaining all the observables for
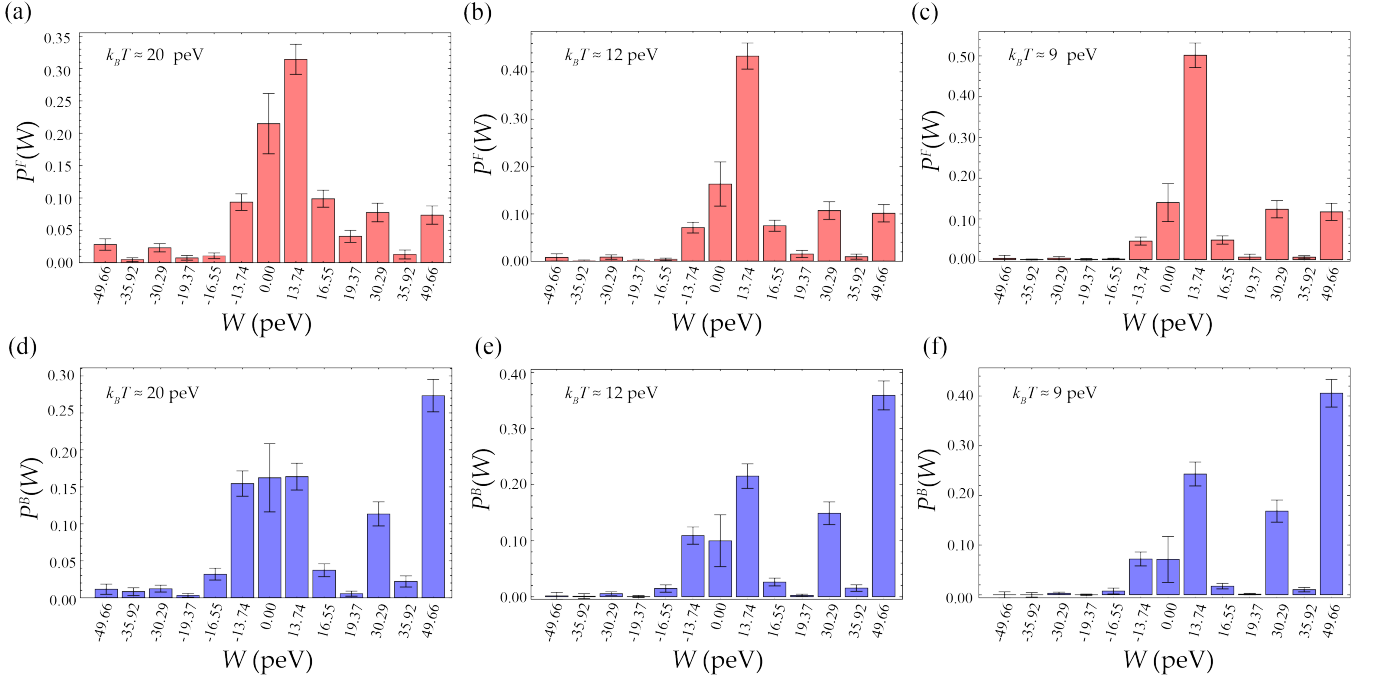
Figure 3. **Experimental result for the the work distribution**. Work distributions for the forward (a,b,c) and backward (d,e,f) protocols for the three different initial spin temperatures (a, d) $k_BT = 20 \pm 3$ peV, (b, e) $k_BT = 12 \pm 2$ peV and (c, f) $k_BT = 9 \pm 2$ peV.

both the forward and backward processes. We note that, depending on the experimental context different observable can be chosen. In the case of an electronic system what would be measured is the local particle density [31].

Due to experimental noise and imperfections, the direct solution from the system of equations could lead to a non physical transition probability matrix. In other words, we could obtain negative values for $p_{m|n}$'s or values greater than one. A similar problem happens in the experimental implementation of quantum state tomography (QST) [37–40], and its source is the fact that different experimental arrangements (measurement apparatus) are needed to measure different observables. Each experimental arrangement carries a particular noise that may lead to nonphysical values. In order to deal with this kind of experimental errors, the Maximum Likelihood Estimation (MLE)[39, 40] method is commonly used for QST. This method requires numerical optimization to generate a definite positive density matrix given a set of experimental data from quantum state tomography. To implement the MLE, a likelihood function is introduced that allows to determine how close the physically estimated density matrix fits the experimental data. Motivated by the successes in quantum state tomography, we propose a MLE method adapted to our problem for obtaining physical transition probabilities for experimental data with noise and imperfections [32].

The obtained statistics for $p_{m|n}$ elements is shown in Fig. 2, where the 16 transition probabilities are identified for both the forward and backward protocols. The experimental transition probabilities obtained from our inversion scheme plus adapted-MLE method [32] and the corresponding theoretical results obtained by direct numerical simulation of the unitary operations in Fig. 1 are in very good agreement for both forward and backward protocols. Also, the validity of the micro-reversibility hypothesis $p_{m|n}^F = p_{n|m}^B$ is satisfied with a good accuracy.

With the method we propose, we can obtain $P(W)$ directly from the results in Fig. 2 and the measurement of the population in the initial thermal state. Experimental results for the work probability distribution are shown in Fig. 3. Transition probabilities between higher energy states are larger for the highest temperature case, with most channels significantly different from zero, than for the lowest temperature cases, where the population of the ground-state is higher: compare Fig. 3(a) and (d) with $k_BT \approx 20$ peV to Fig. 3(c) and (f), where $k_BT \approx 9$ peV. To highlight the importance of interactions, we compare in [32] the experimental results for the work distribution to its theoretical interacting and non-interacting counterparts.

Using our protocol we can also verify the detailed fluctuation relation [5, 6, 8]

$$\frac{P^F(+W)}{P^B(-W)} = e^{(W-\Delta F)/(k_BT)}, \tag{3}$$

for this interacting spins system driven out-of-equilibrium. Here ΔF is the free energy variation. In
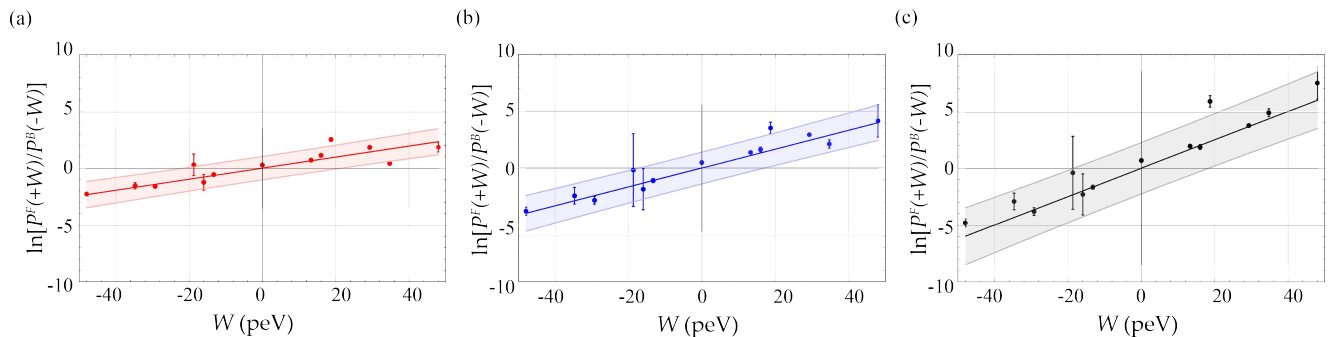
Figure 4. **Detailed fluctuation relation for two interacting spin 1/2.** The experimental results and the linear fit for the logarithm of the detailed fluctuation relation, $\ln\left[P^F\left(+W\right)/P^B\left(-W\right)\right] = W\left(k_B T\right)^{-1}$, are displayed for three different initial-state-preparation temperatures: (a) $k_B T = 20 \pm 3$ peV, (b) $k_B T = 12 \pm 2$ peV and (c) $k_B T = 9 \pm 2$ peV. The highlighted areas between the thin lines in the panels represent the prediction interval where an observation could fall with confidence level of 99%. The linear regression is performed excluding these out-layer points: $W = \pm 19.37$peV for all panels and also $W = 35.92$ peV for panel (a). The resulting temperatures are: (a) $k_B T = 21 \pm 2$ peV, (b) $k_B T = 12 \pm 1$ peV, and (c) $k_B T = 8 \pm 1$ peV [32].

our experiment $\Delta F = 0$, since the Hamiltonian after and before the driving protocol are the same. In Fig. 4 we show the logarithm of Eq. (3) for the three different temperatures. The points represent the experimental result. The solid line is the linear regression for each spin temperature data set and, from Eq. (3), the slope of each line gives an estimate of the corresponding inverse temperature $(k_B T)^{-1}$. The estimated error of each point is obtained by means of standard error propagation. The temperatures estimated in this way are in good agreement with the temperatures of the initial Gibbs states certified by QST [32].

Conclusions. To summarize, we have proposed and experimentally implemented a new approach to access energy fluctuations and the work distribution in a many body quantum system. We have tested our method in an Ising-like system composed by two spin-1/2 and driven out-of-equilibrium. In addition, by obtaining the bi-stochastic transition probability matrix for the system dynamics at different temperatures, we were able to verify the detailed quantum fluctuation relation for an interacting system. The method introduced here can be applied in a diversity of physical setups to investigate energy fluctuations and thermodynamical quantities such as, work, heat, and entropy production in non-equilibrium quantum systems.

* Electronic Address: amherrera@uao.edu.co
† Electronic Address: serra@ufabc.edu.br
‡ Electronic Address: irene.damico@york.ac.uk

[1] J. Goold, M. Huber, A. Riera, L. del Rio, and P. Skrzypczyk, The role of quantum information in thermodynamics – a topical review, J. Phys. A: Math. Theor. **49**, 143001 (2016).
[2] S. Vinjanampathy and J. Anders, Quantum thermodynamics, Contemp. Phys. **57**, 545 (2016).
[3] R. Kosloff, Quantum Thermodynamics: A Dynamic Viewpoint, Entropy **15**, 2100 (2013).
[4] C. Jarzynski, Nonequilibrium Equality for Free Energy Differences, Phys. Rev. Lett. **78**, 2690 (1997).
[5] G. E. Crooks Entropy Production Fluctuation Theorem and the Nonequilibrium Work Relation for Free-Energy Differences, Phys. Rev. E **60**, 2721 (1999).
[6] J. Kurchan, A quantum fluctuation theorem, cond-mat/0007360; H. Tasaki, and C. Jarzynski, Relations for Quantum Systems and Some Applications, cond-mat/0009244v2.
[7] S. Mukamel, Quantum extension of the Jarzynski relation: Analogy with stochastic dephasing, Phys. Rev. Lett. **90**, 170604 (2003).
[8] P. Talkner, and P. Hänggi, The Tasaki-Crooks quantum fluctuation theorem, J. Phys. A **40**, F569 (2007).
[9] M. Esposito, U. Harbola, and S. Mukamel, non-equilibrium fluctuations, fluctuation theorems, and counting statistics in quantum systems, Rev. Mod. Phys. **81**, 1665 (2009).
[10] M. Campisi, P. Hänggi, and P. Talkner, Colloquium: Quantum fluctuation relations: Foundations and applications, Rev. Mod. Phys. **83**, 771 (2011).
[11] P. Hänggi and P. Talkner, The other QFT, Nat. Phys. **11**, 108 (2015).
[12] P. A. Camati and R. M. Serra, Verifying detailed fluctuation relations for discrete feedback-controlled quantum dynamics, Phys. Rev. A **97**, 042127 (2018).
[13] R. Dorner, S.R. Clark, L. Heaney, R. Fazio, J. Goold, and V. Vedral, Extracting quantum work statistics and

fluctuation theorems by single-qubit interferometry, Phys. Rev. Lett. **110**, 230601 (2013).

[14] L. Mazzola, G. De Chiara, and M. Paternostro, Measuring the characteristic function of the work distribution, Phys. Rev. Lett. **110**, 230602 (2013).

[15] T. B. Batalhão, A. M. Souza, L. Mazzola, R. Auccaise, R. S. Sarthour, I. S. Oliveira, J. Goold, G. De Chiara, M. Paternostro, and R. M. Serra, Experimental Reconstruction of Work Distribution and Study of Fluctuation Relations in a Closed Quantum System, Phys. Rev. Lett. **113**, 140601 (2014).

[16] T. B. Batalhão, A. M. Souza, R. S. Sarthour, I. S. Oliveira, M. Paternostro, E. Lutz, R. M. Serra, Irreversibility and the Arrow of Time in a Quenched Quantum System. Phys. Rev. Lett. **115**, 190601 (2015).

[17] P. A. Camati, J. P. S. Peterson, T. B. Batalhão, K. Micadei, A. M. Souza, R. S. Sarthour, I. S. Oliveira, and R. M. Serra, Experimental Rectification of Entropy Production by Maxwell's Demon in a Quantum System, Phys. Rev. Lett. **117**, 240502 (2016).

[18] J. P. S. Peterson, T. B. Batalhão, M. Herrera, A. M. Souza, R. S. Sarthour, I. S. Oliveira, R. M. Serra, Experimental characterization of a spin quantum heat engine, Phys. Rev. Lett. **123**, 240601 (2019).

[19] F. Cerisola, Y. Margalit, S. Machluf, A. J. Roncaglia, J. P. Paz and R. Folman , Using a quantum work meter to test non-equilibrium fluctuation theorems, Nat. Commun. **8**, 1241 (2017).

[20] R. O. Jones, Density functional theory: Its origins, rise to prominence, and future, Rev. Mod. Phys. 87, 897 (2015).

[21] M. Herrera, R. M. Serra, and I. D'Amico, Scientific reports **7**, 4655 (2017)

[22] M. Herrera, K. Zawadzki, and I. D'Amico, Eur. Phys. J. B **91**, 248 (2018)

[23] A. H. Skelt, K. Zawadzki and I. D'Amico, J. Phys. A: Math. Theor. 52, 485304 (2019)

[24] P. Talkner, E. Lutz, and P. Hänggi, Fluctuation theorems: Work is not an observable, Phys. Rev. E **75**, 050102(R) (2007).

[25] P. Talkner and P. Hänggi, Aspects of quantum work, Phys. Rev. E **93**, 022131 (2016).

[26] U. Seifert, Stochastic thermodynamics, fluctuation theorems and molecular machines, Rep. Prog. Phys. **75**, 126001 (2012).

[27] S. Suomela, P. Solinas, J. P. Pekola, J. Ankerhold, and T. Ala-Nissila, Phys. Rev. B **90**, 094304 (2014).

[28] T. Monnai, Unified treatment of the quantum fluctuation theorem and the Jarzynski equality in terms of microscopic reversibility, Phys. Rev. E **72**, 027102 (2005).

[29] G. Watanabe, B. P. Venkatesh, and P. Talkner, Generalized energy measurements and modified transient quantum fluctuation theorems, Phys. Rev. E **89**, 052116 (2014).

[30] A. J. Roncaglia, F. Cerisola, and J. P. Paz, Work measurement as a generalized quantum measurement, Phys. Rev. Lett. **113**, 250601 (2014).

[31] N. Rohringer, S. Peter, and J. Burgdorfer, Calculating state-to-state transition probabilities within time-dependent density-functional theory, Phys. Rev. A **74**, 042512 (2006).

[32] See Supplemental Material for more details.

[33] S. An, J.-N. Zhang, M. Um, D. Lv, Y. Lu, J. Zhang, Z.-Q. Yin, H. Quan, and K. Kim, Nat. Phys. **11**, 193 (2014).

[34] J. P. Peterson, R. S. Sarthour, A. M. Souza, I. S. Oliveira,

J. Goold, K. Modi, D. O. Soares-Pinto, and L. C. Celeri, Proc. R. Soc. A **472**, 20150813 (2016).

[35] I. S. Oliveira, T. J. Bonagamba, R. S. Sarthour, J. C. C. Freitas, and R. R. deAzevedo, NMR Quantum Information Processing (Elsevier, Amsterdam, 2007).

[36] F. Vatan and C. Williams, Optimal quantum circuits for general two-qubit gates, Phys. Rev. A **69**, 032315 (2004).

[37] I. L. Chuang and M. A. Nielsen, Prescription for experimental determination of the dynamics of a quantum black box, J. Mod. Opt. **44**, 2455 (1997).

[38] M. A. Nielsen and I. L. Chuang, *Quantum Computation and Quantum Information* (Cambridge University Press, 2011).

[39] K. Banaszek, G. M. A. D'Ariano, M. G. Paris, and M. F. Sacchi, Maximum-likelihood estimation of the density matrix, Phys. Rev. A **61**, 010304 (1999).

[40] D. F. V. James, P. G. Kwiat, W. J. Munro, and A. G. White, Measurement of qubits, Phys. Rev. A **64**, 052312 (2001).

[41] K. Micadei, J. P. S. Peterson, A. M. Souza, R. S. Sarthour, I. S. Oliveira, G. T. Landi, T. B. Batalhão, R. M. Serra, and E. Lutz, Reversing the direction of heat flow using quantum correlations, Nat. Commun. **10**, 2456 (2019).

[42] We note that instead the strength of many-body interactions *within* the system does not restrict the protocol speed.

[43] In principle one could apply the method even if $\mathcal{O}$ and $\mathcal{H}_\tau$ would not commute, however this would require many more measurements. Depending on the specific experimental scenario, our method can be adapted according to the available observables and range of temperatures.

SUPPLEMENTAL MATERIAL

We provide here supplementary details about the experimental setup, data analysis, and extensions to large systems.

EXPERIMENTAL SETUP

For the implementation of the method and characterization of the energy fluctuations, we employed a ^{13}C-labeled CHCl$_3$ liquid sample and a 500 MHz Varian NMR spectrometer. The nuclear spins of the ^{1}H and ^{13}C atoms of this molecule can be used to represent a two-qubit system. The Hamiltonian of this system is composed by an interaction term $\mathcal{H}_{int}$ that represents thel interaction between ^{1}H and ^{13}C nuclei in the molecule and a term $\mathcal{H}_Z$ which expresses the interaction with the external magnetic fields [35]. The interaction term is mainly due to the scalar coupling between the Carbon and Hydrogen nuclear spin that reads

$$\mathcal{H}_{int} = \frac{1}{4}hJ\sigma_z^H\sigma_z^C, \tag{S1}$$

where $J \approx 215.1$ Hz is the coupling constant. For performing NMR experiments, the sample is placed inside of a superconducting magnet where it is produced a strong static magnetic field $\boldsymbol{B}_0 \approx 11.75\ T$. The interaction between the nuclear spins and this magnetic field aligned along the z-axis induces the Zeeman effect with a Larmor frequency of $\upsilon_n = -\gamma_n B_0$, where γ_n is the gyromagnetic factor characteristic for each nuclear species [35]. In oder to set correctly the resonance frequency of both nuclei, the chemical shift should be also considered [35]. Including the chemical shift, the interaction with the magnetic field can be described by the Hamiltonian

$$\mathcal{H}_Z = -\frac{1}{2}h\nu_H\sigma_z^H - \frac{1}{2}h\nu_C\sigma_z^C, \tag{S2}$$

where ν_H and ν_C are the resonance frequencies [35] of the Hydrogen and Carbon nuclei, respectively. To describe the dynamics of the nuclear spins, it is used a rotating frame that moves around the z-direction with a traverse frequency offset ν_{rf}, in such frame we obtain the effective Hamiltonian [35]

$$\mathcal{H}' = -\frac{1}{2}h\left(\nu_H - \nu_{rf}\right)\sigma_z^H - \frac{1}{2}h\left(\nu_C - \nu_{rf}\right)\sigma_z^C + \frac{1}{4}hJ\sigma_z^H\sigma_z^C. \tag{S3}$$

An important ingredient to perform our experiments is the initialization of the system. A relevant feature in the NMR experiments is that it is not possible to deal with a single molecule but with samples containing an ensemble of many identical molecules, each with the relevant
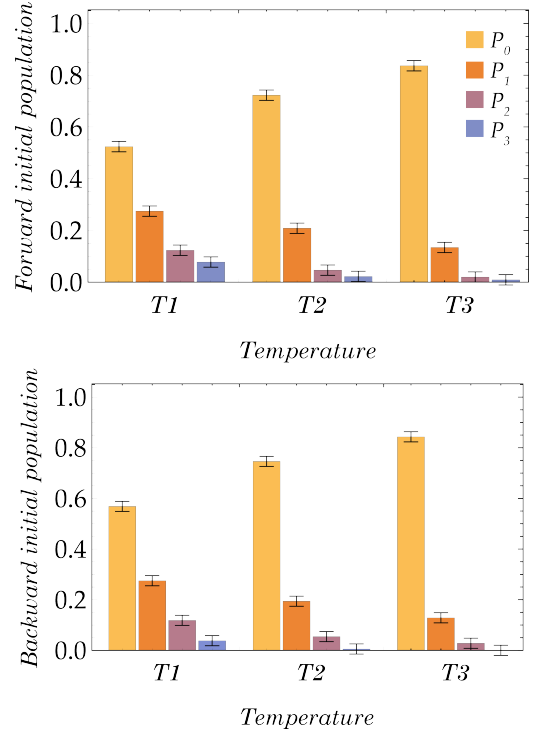

Figure S1. Populations of the initial state for all effective-spin-temperatures considered.

nuclear spins (qubits). In particular, for the experiment presented here we have used liquid samples highly diluted in deuterated acetone. This ensures us that we will have an ensemble of non-interacting molecules, which means that we have many copies of the same system. For the implementation of our protocol, we wish to start from thermal states, which are diagonal in the Hamiltonian basis. Our sample is initially prepared in thermal-like states corresponding to different spin-temperatures T and such states can be characterized using a full quantum state tomography [1].

The initial population distribution of the system (corresponding to a thermal Gibbs state) is shown in Fig. S1 for both the forward and backward protocols. Using these populations we can estimate the effective spin temperature of the initial pseudo thermal state by means of the expression $k_B T = (E_2 - E_0)/\ln\left(\frac{p_0}{p_2}\right)$, where $E_2 - E_0$ is the energy difference between the ground state and the second excited state. These spin temperatures are reported in Table SI.

We implement the forward $\mathcal{U}_F$ and backwards $\mathcal{U}_B$ evolutions, by applying the unitary operations depicted in the pulse sequences of Fig. 1 with the angles display in Table SII

$k_B T$ (peV)			
	Forward	Backward	Average	fluctuation relation
$k_B T_1$	21±3	19±3	20±3	21±2
$k_B T_2$	11±2	12±2	12±2	12±1
$k_B T_3$	8±2	9±2	9±2	8±1

Table SI. Characterization of the initial state temperature for the forward and backward protocol. The effective spin temperature of the prepared state is estimated from the populations as $k_B T = (E_2 - E_0) / \ln\left(\frac{p_0}{p_2}\right)$, for this experiment $E_2 - E_0 = 30.3$ peV.

i	1	2	3	4	5	6
α_i (rad)	0.48	-0.80	$\pi/2$	-3.61	0.69	$\pi/2$
γ_i (rad)	-0.83	1.40	$\pi/2$	-3.65	2.68	$\pi/2$

Table SII. Parameters used in the pulse sequence displayed in figure 1 on the main text.

MAGNETIZATION AND CORRELATION MEASUREMENTS

After applying experimentally the protocols that we have described in the Letter, we measure the magnetization. The obtained values are reported in Table SIII. As we can see, the experimental values are very close to expected theoretical values. However the influence of experimental imperfections and the uncontrolled coupling with the environment is the reason we can observe some deviations. These imperfections affect the statistics of the system and therefore the transition probabilities: this is why we have to apply the Maximum Likelihood Estimation (MLE) adapted for such probabilities, as presented in the following section.

MAXIMUM LIKELIHOOD ESTIMATION TO OBTAIN TRANSITION PROBABILITIES

For our experiment we measured the magnetization of each nuclear spin $\langle \sigma_z^H \rangle$, $\langle \sigma_z^C \rangle$ and the correlation function $\langle \sigma_z^H \sigma_z^C \rangle$ at three different spin temperatures. Using

$$\langle \mathcal{O}(\tau) \rangle = \sum_{m,n} \mathcal{O}_m p_n^0 p_{m|n} \tag{S4}$$

(see main text) the expression of these mean values are given by

$$\langle \sigma_z^H \rangle (\beta) = 2 \sum_n^{N-1} \left(p_n^\beta - p_4^\beta \right) p_{1|n} + \sum_n^{N-1} \left(p_n^\beta - p_4^\beta \right) p_{3|n} + 2p_4^\beta - 1, \tag{S5}$$

$$\langle \sigma_z^C \rangle (\beta) = 2 \sum_n^{N-1} \left(p_n^\beta - p_4^\beta \right) p_{1|n} + \sum_n^{N-1} \left(p_n^\beta - p_4^\beta \right) p_{2|n} + 2p_4^\beta - 1, \tag{S6}$$

$$\langle \sigma_z^H \sigma_z^C \rangle (\beta) = -2 \sum_n^{N-1} \left(p_n^\beta - p_4^\beta \right) p_{2|n} - \sum_n^{N-1} \left(p_n^\beta - p_4^\beta \right) p_{3|n} - 2p_4^\beta + 1. \tag{S7}$$

Effective temperature 1			
	Experiment		Theory	
	Forward	Backward	Forward	Backward
$\langle \sigma_z^H \rangle$	0.13±0.05	-0.14±0.05	0.15	-0.16
$\langle \sigma_z^C \rangle$	-0.20±0.05	0.07±0.05	-0.19	0.07
$\langle \sigma_z^H \sigma_z^C \rangle$	-0.26±0.05	0.13±0.05	-0.27	0.11

Effective temperature 2			
	Experiment		Theory	
	Forward	Backward	Forward	Backward
$\langle \sigma_z^H \rangle$	0.26±0.05	-0.28±0.05	0.30	-0.31
$\langle \sigma_z^C \rangle$	-0.32±0.05	0.04±0.05	-0.32	0.01
$\langle \sigma_z^H \sigma_z^C \rangle$	-0.39±0.05	0.18±0.05	-0.36	0.18

Effective spin temperature 3			
	Experiment		Theory	
	Forward	Backward	Forward	Backward
$\langle \sigma_z^H \rangle$	0.34±0.05	-0.38±0.05	0.41	-0.42
$\langle \sigma_z^C \rangle$	-0.37±0.05	0.01±0.05	-0.39	-0.05
$\langle \sigma_z^H \sigma_z^C \rangle$	-0.44±0.05	0.17±0.05	-0.39	0.20

Table SIII. Values of the magnetization and correlation function.

Using the expression of the mean values (S5), (S6), and (S7) we construct the matrix equation $\mathcal{A}\boldsymbol{x} = \boldsymbol{b}$ as explained in the main letter (see Eq. (1) of the main text).

$$
\begin{bmatrix}
2\sum_n^{N-1}\left(p_n^{\beta_1}-p_4^{\beta_1}\right)p_{1|n}+\sum_n^{N-1}\left(p_n^{\beta_1}-p_4^{\beta_1}\right)p_{3|n}+2p_4^{\beta_1}-1 \\
2\sum_n^{N-1}\left(p_n^{\beta_1}-p_4^{\beta_1}\right)p_{1|n}+\sum_n^{N-1}\left(p_n^{\beta_1}-p_4^{\beta_1}\right)p_{2|n}+2p_4^{\beta_1}-1 \\
-2\sum_n^{N-1}\left(p_n^{\beta_1}-p_4^{\beta_1}\right)p_{2|n}-\sum_n^{N-1}\left(p_n^{\beta_1}-p_4^{\beta_1}\right)p_{3|n}-2p_4^{\beta_1}+1 \\
2\sum_n^{N-1}\left(p_n^{\beta_2}-p_4^{\beta_2}\right)p_{1|n}+\sum_n^{N-1}\left(p_n^{\beta_2}-p_4^{\beta_2}\right)p_{3|n}+2p_4^{\beta_2}-1 \\
2\sum_n^{N-1}\left(p_n^{\beta_2}-p_4^{\beta_2}\right)p_{1|n}+\sum_n^{N-1}\left(p_n^{\beta_2}-p_4^{\beta_2}\right)p_{2|n}+2p_4^{\beta_2}-1 \\
-2\sum_n^{N-1}\left(p_n^{\beta_2}-p_4^{\beta_2}\right)p_{2|n}-\sum_n^{N-1}\left(p_n^{\beta_2}-p_4^{\beta_2}\right)p_{3|n}-2p_4^{\beta_2}+1 \\
2\sum_n^{N-1}\left(p_n^{\beta_3}-p_4^{\beta_3}\right)p_{1|n}+\sum_n^{N-1}\left(p_n^{\beta_3}-p_4^{\beta_3}\right)p_{3|n}+2p_4^{\beta_3}-1 \\
2\sum_n^{N-1}\left(p_n^{\beta_3}-p_4^{\beta_3}\right)p_{1|n}+\sum_n^{N-1}\left(p_n^{\beta_3}-p_4^{\beta_3}\right)p_{2|n}+2p_4^{\beta_3}-1 \\
-2\sum_n^{N-1}\left(p_n^{\beta_3}-p_4^{\beta_3}\right)p_{2|n}-\sum_n^{N-1}\left(p_n^{\beta_3}-p_4^{\beta_3}\right)p_{3|n}-2p_4^{\beta_3}+1
\end{bmatrix}
=
\begin{bmatrix}
\langle\sigma_z^H\rangle(\beta_1) \\
\langle\sigma_z^C\rangle(\beta_1) \\
\langle\sigma_z^H\sigma_z^C\rangle(\beta_1) \\
\langle\sigma_z^H\rangle(\beta_2) \\
\langle\sigma_z^C\rangle(\beta_2) \\
\langle\sigma_z^H\sigma_z^C\rangle(\beta_2) \\
\langle\sigma_z^H\rangle(\beta_3) \\
\langle\sigma_z^C\rangle(\beta_3) \\
\langle\sigma_z^H\sigma_z^C\rangle(\beta_3)
\end{bmatrix}
\tag{S8}
$$

It is important to stress that if the measured data were perfect (without any noise), as in a numerical simulation, the method leads directly to the correct result. However due to experimental noise, the direct solution of the Eq. (S8) from the experimental data could yield to nonphysical results. We can overcome this problem by searching in all the possible valid solutions (in the sense of the set of transition probabilities obtained being a valid bistochastic matrix) and extract the closest physical probabilities that solve Eqs. (S8). Those physical probabilities in general will not reproduce exactly the measured data, but they will be the most likely to produce the experimental observation. A similar problem occurs in quantum state tomography. Here, the usual procedure to apply the MLE is to use a particular representation for the density matrix given by

$$
\rho = \frac{\mathcal{T}\mathcal{T}^\dagger}{\mathrm{Tr}\left(\mathcal{T}\mathcal{T}^\dagger\right)}, \tag{S9}
$$

where $\mathcal{T}$ is a triangular matrix. Equation (S9) guarantees that the density matrix will be a Hermitian defined positive matrix with trace one. For example, considering a system with two qubits, we can write $\mathcal{T}$ as

$$
\mathcal{T} = \begin{pmatrix}
t_1 & 0 & 0 & 0 \\
t_5+it_6 & t_2 & 0 & 0 \\
t_7+it_8 & t_9+it_{10} & t_3 & 0 \\
t_{11}+it_{12} & t_{13}+it_{14} & t_{15}+it_{16} & t_4
\end{pmatrix}, \tag{S10}
$$

where t_i are the parameters that have to be defined in the optimization of the maximum likelihood function given the experimental data set.

However, for a transition probability matrix, things are more complicated. For a transition probability matrix P, one could think to resort to the Birkhoff–von Neumann decomposition [2]. This states that for a bistochastic matrix P – i.e. $\sum_m P_{m|n} = \sum_n P_{m|n} = 1$ – there exist the parameters θ_1, θ_2,...,$\theta_k \in (0,1)$ with $\sum_{j=}^k \theta_j = 1$ and the permutation matrices Λ_1, Λ_2,...,Λ_k such that P

can be decomposed as

$$
P = \theta_1\Lambda_1 + \theta_2\Lambda_2 + \ldots + \theta_k\Lambda_k. \tag{S11}
$$

A permutation matrix Λ_j is a square matrix whose rows and columns contain exactly one nonzero entry, which is 1. However this representation may, in general, not be unique, and finding the representation with the minimum number of terms has been shown to be NP-hard problem [2]. Due to the difficulty of using such a representation we are going to use a different approach and instead of defining a specific representation for the transition probability matrix, we will solve Eq. (S8). From that solution and by means of the numerical optimizations explained below, we will obtain the closest physical solution.

Based on this, we define our likelihood function as

$$
\mathcal{F}(x) = \sum_{k,j}\left(x_{k,j}-\Xi_{k,j}\right)^2, \tag{S12}
$$

where $x_{k,j}$ are the solution of the system of equations given in (S8) as constructed from the set of the experimentally measured observables, and Ξ is a positive matrix, whose elements satisfy the condition $0 \leq \Xi_{k,j} \leq 1$. Then, we find the minimum of Eq. (S12) to obtain the closest positive matrix Ξ that better fit our expected result. Doing the minimization we only guarantee that the elements of the optimized matrix are probabilities, but such elements also have to satisfy the constraint $\sum_k \Xi_{k,j} = \sum_j \Xi_{k,j} = 1$. We can transform the positive matrix Ξ into a bistochastic one using the Sinkhorn-Knopp algorithm [3]. That algorithm is a simple iterative method that generates a bistochastic matrix by alternatively normalizing the rows and the columns of a positive matrix. After getting the bistochastic matrix by the application of the Sinkhorn-Knopp algorithm, we repeat the minimization by using the likelihood function (S12) where this solution enters in the next cycle as a new $\Xi_{k,j}$ and start the process over again until finally we reach a convergence in the final solution. For our calculation we

are setting a threshold of 1000 iteration with a tolerance of 1×10^{-6}, but the convergence of this protocol is fast, for the forward protocol we needed 3 iterations and for the backward protocol 13 iterations only.

SYSTEMS LARGER THAN FEW BODIES

A. Initial state

The reconstruction of the system's initial quantum state is not strictly necessary at the beginning of the protocol. Quantum state tomography (QST) for the initial state can in fact be avoided as long as it can be reasonably assumed that the initial state is known, e.g. because the system has been carefully prepared in a desired state or has been allowed to thermalize at a known temperature.

In addition, for large systems, there are by now several methods which significantly improve on the scaling of QST with system size, making its scaling less than exponential or providing a good approximation for the state. Possibilities are, for instance, compressed sensing QST [5], quantum state learning [6], QST assisted by machine learning [7].

B. Adapting the method to large systems

1. Systems described by a lattice Hamiltonian

For lattice systems, the operators to be measured to derive the work distribution function should be chosen based on what is easy to measure for the specific system at hand. However, for systems bigger than few-bodies, the number of transitions would become prohibitively large to be reconstructed one-by-one, by this – and possibly any other – method. In this case it is suggested to use an interpolation approach within the proposed method to reconstruct the work distribution.

For large many-body systems, the number of transitions increases rapidly with size: we expect then the work probability distribution to regularise very rapidly to a fairly well-defined bell shape. Indeed, we observed this already for systems of the order of 6-8 spins [8]. In this case, it would be superfluous to measure this curve for every single transition, while a coarse-grained sampling would be sufficient to reconstruct the curve. The solution of Eq. (1) in our paper could then be adapted to the case in which a simple continuous function is assumed for the distribution. The same approximated methods for QST for large systems mentioned in the previous subsection could be adapted to solve this problem.

An interesting case would be the one of very strongly correlated systems. In this case correlations reduce – de facto – the Hilbert space to very few allowed transitions, as seen for example in Fig. 1 (b) and (d) in Ref. [8]. Here the original scheme as currently described in the paper could be used.

2. Continuous, interacting N-particle systems

Within the context of density functional theory (DFT), Ref. [31] proposed two functionals for the transition matrix $p_{m|n}$ and discussed their limitations. These functionals are derived via an inversion scheme, and their key ingredient is the time-dependent electronic local density. More recently, Ref. [9] proposed a way to access energy fluctuations in scale-invariant, continuous quantum fluids. In the following, we highlight how our method can be adapted to systems of continuous variables.

For continuous, interacting N-particle systems, the measure of a single local operator which commutes with the final Hamiltonian H_τ is in principle sufficient to determine the transition matrix $p_{m|n}$ and hence the work probability distribution.

In this case we can write Eq. (S4) as

$$\mathcal{O}(\mathbf{r}, \tau) = \text{Tr}[\hat{O}(\mathbf{r})\hat{\rho}(t)] \tag{S13}$$

$$= \sum_{m,n}^{M} \mathcal{O}(\mathbf{r})_m p_n^0 p_{m|n}, \tag{S14}$$

where both $\mathcal{O}(\mathbf{r}, \tau)$, and $\mathcal{O}(\mathbf{r})_m$ are local and measurable. For example, where appropriate, $\mathcal{O}(\mathbf{r}, \tau)$ could be the local particle density $n(\mathbf{r}, \tau)$ or the local magnetization $m(\mathbf{r}, \tau)$. For electronic systems, the advantage of these observables is that good estimates of them could be calculated using DFT, which could facilitate the inversion scheme.

Because the system is continuous, there is, in principle, no limit to the number of points $\mathbf{r}$ where these measurements could be taken, and hence the measurement of a single local operator is enough to recover all elements of the matrix $p_{m|n}$. A more practical approach would be to perform measurements over a manageable set of points $(\mathbf{r}_1, \mathbf{r}_2, \ldots \mathbf{r}_s)$ and then fit the sets of measurements to continuous functions. In addition, for electronic systems, DFT methods [4] could be used to get approximations for $p_{m|n}$, which could aid the inversion scheme.

In electronic systems, the number of eigenstates M is generally very large, for all practical purposes infinite. This could be tackle by truncating the basis appropriately with respect to the characteristic energies (including the spin temperature) of the system at hand.

We aim to explore these points further in future developments of the method.

COMPARISON BETWEEN EXPERIMENTAL RESULTS AND THEORETICAL SIMULATIONS FOR THE FORWARD AND BACKWARD STROKE WORK DISTRIBUTION

We are reporting in this section the comparison between the experimentally extracted work distributions in Fig. 3 of the main text with the corresponding theoretical simulations, for both the forward (Fig. S2) and the backward (Fig. S3) process. The technical imprecision is associated to the errors bars in the experimental data. Indeed, these figures confirms the very good agreement between the theoretical predictions and results from the experiment, with the great majority of experimentally extracted work probabilities being well within one error bar of the predicted results.

COMPARISON BETWEEN EXPERIMENTAL RESULTS AND THE CORRESPONDING NON-INTERACTING THEORETICAL SYSTEM FOR THE FORWARD AND BACKWARD STROKE WORK DISTRIBUTION

We are reporting in this section the comparison between the experimentally extracted work distributions in Fig. 3 of the main text and the simulations' results for the corresponding non-interacting system ($J = 0$), for both the forward (Fig. S4) and the backward (Fig. S5) process. As can be observed the non-interacting results are qualitatively and quantitatively distinct from the experimental ones, underlying the importance of interactions at the temperatures considered.

* Electronic Address: amherrera@uao.edu.co
† Electronic Address: serra@ufabc.edu.br
‡ Electronic Address: irene.damico@york.ac.uk

[1] I. S. Oliveira, T. J. Bonagamba, R. S. Sarthour, J. C. C. Freitas, and R. R. deAzevedo, NMR Quantum Information Processing (Elsevier, Amsterdam, 2007)

[2] F. Dufossé and B. Uçar, Notes on Birkhoff-von Neumann decomposition of doubly stochastic matrices, Linear Algebra Appl. **497**, 108 (2016).

[3] R. Sinkhorn and P. Knopp, Concerning nonnegative matrices and doubly stochastic matrices, Pacic J. Math. **21**, 343 (1967).

[4] N. Rohringer, S. Peter, and J. Burgdorfer, Calculating state-to-state transition probabilities within time-dependent density-functional theory, Phys. Rev. A **74**, 042512 (2006).

[5] Anastasios Kyrillidis, Amir Kalev, Dohyung Park, Srinadh Bhojanapalli, Constantine Caramanis, Sujay Sanghavi, Provable compressed sensing quantum state tomography via non-convex methods, NPJ Quantum Information **4**, 36 (2018); A Steffens, C A Riofrío, W McCutcheon, I Roth, B A Bell, A McMillan, M S Tame, J G Rarity and J Eisert, Experimentally exploring compressed sensing quantum tomography, Quantum Sci. Technol. **2**, 025005 (2017).

[6] A. Rocchetto, S. Aaronson, S. Severini, G. Carvacho, D. Poderini, I. Agresti, M. Bentivegna, and F. Sciarrino, Experimental learning of quantum states, Sci. Adv. **5**, eaau1946 (2019).

[7] Sanjaya Lohani, Brian T Kirby, Michael Brodsky, Onur Danaci and Ryan T Glasser, Machine learning assisted quantum state estimation, Mach. Learn.: Sci. Technol. **1**, 035007 (2020)

[8] Krissia Zawadzki, Roberto M. Serra, and Irene D'Amico, Work-distribution quantumness and irreversibility when crossing a quantum phase transition in finite time, Phys. Rev. Research **2**, 033167 (2020).

[9] Mathieu Beau and Adolfo del Campo, Nonadiabatic Energy Fluctuations of Scale-Invariant Quantum Systems in a Time-Dependent Trap, Entropy **22**, 515 (2020).
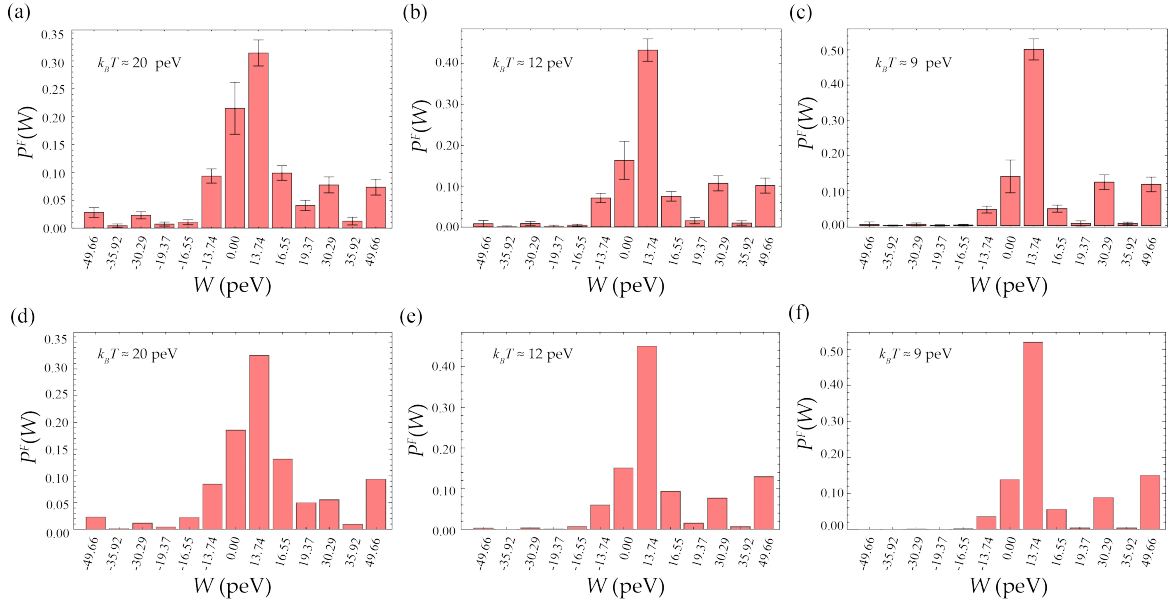
1

Figure S2. Experimental (a, b, c) and theoretical (d, e, f) results for the forward work distribution for the three different initial spin temperatures (a, d) $k_BT = 20 \pm 3$ peV, (b, e) $k_BT = 12 \pm 2$ peV and (c, f) $k_BT = 9 \pm 2$ peV
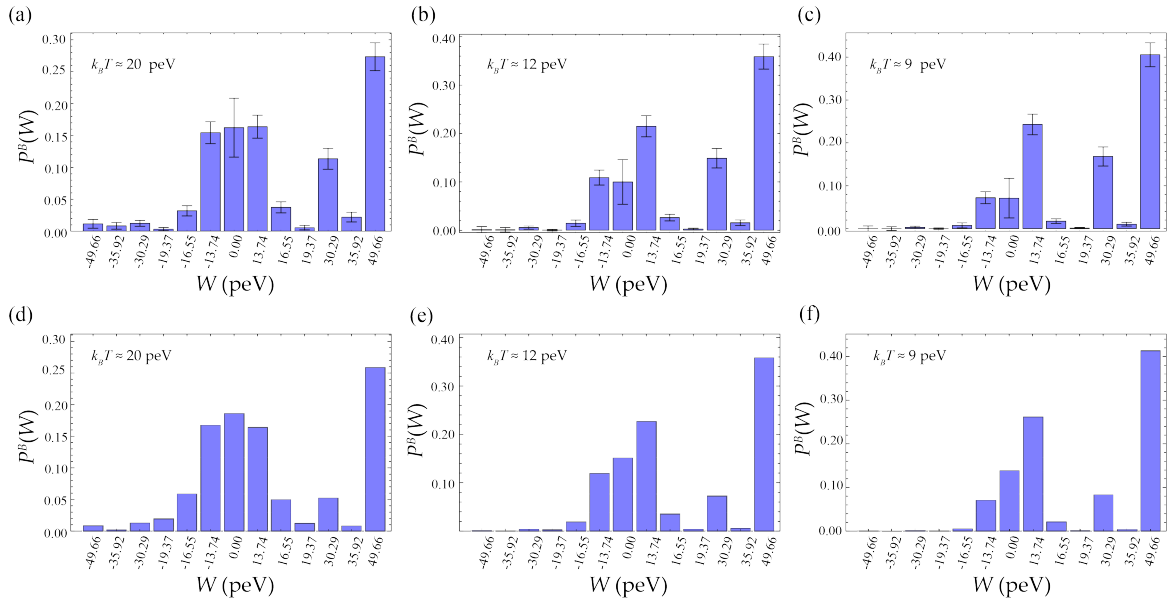
.

Figure S3. Experimental (a, b, c) and theoretical (d, e, f) results for the backward work distribution for the three different initial spin temperatures (a, d) $k_BT = 20 \pm 3$ peV, (b, e) $k_BT = 12 \pm 2$ peV and (c, f) $k_BT = 9 \pm 2$ peV.
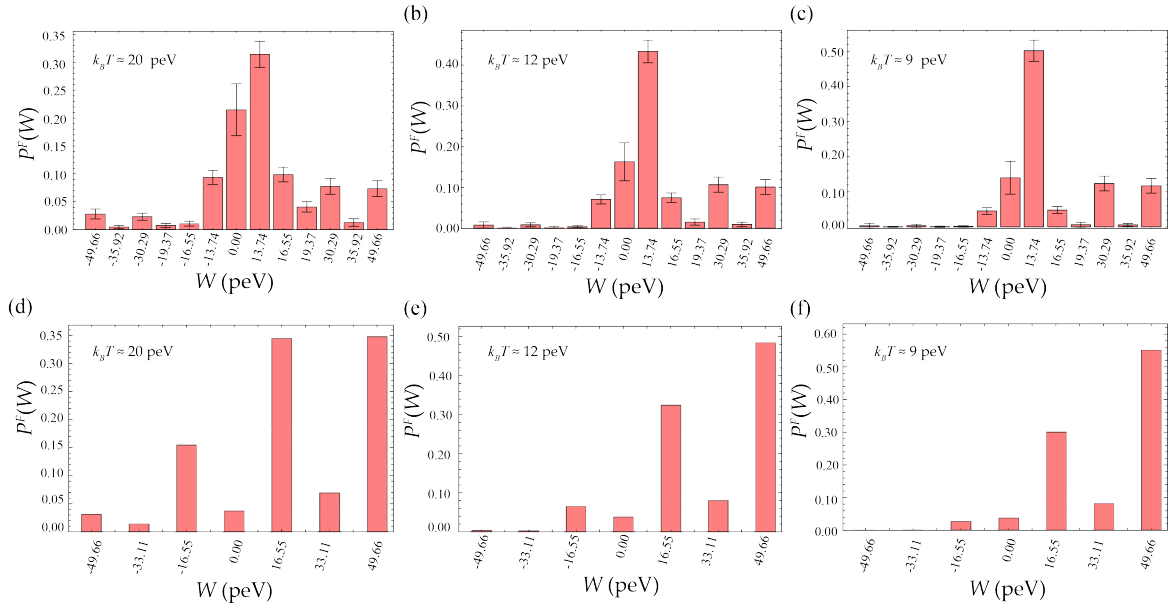
Figure S4. Experimental (a, b, c) and non-interacting theoretical (d, e, f) results for the forward work distribution for the three different initial spin temperatures (a, d) $k_BT = 20 \pm 3$ peV, (b, e) $k_BT = 12 \pm 2$ peV and (c, f) $k_BT = 9 \pm 2$ peV.
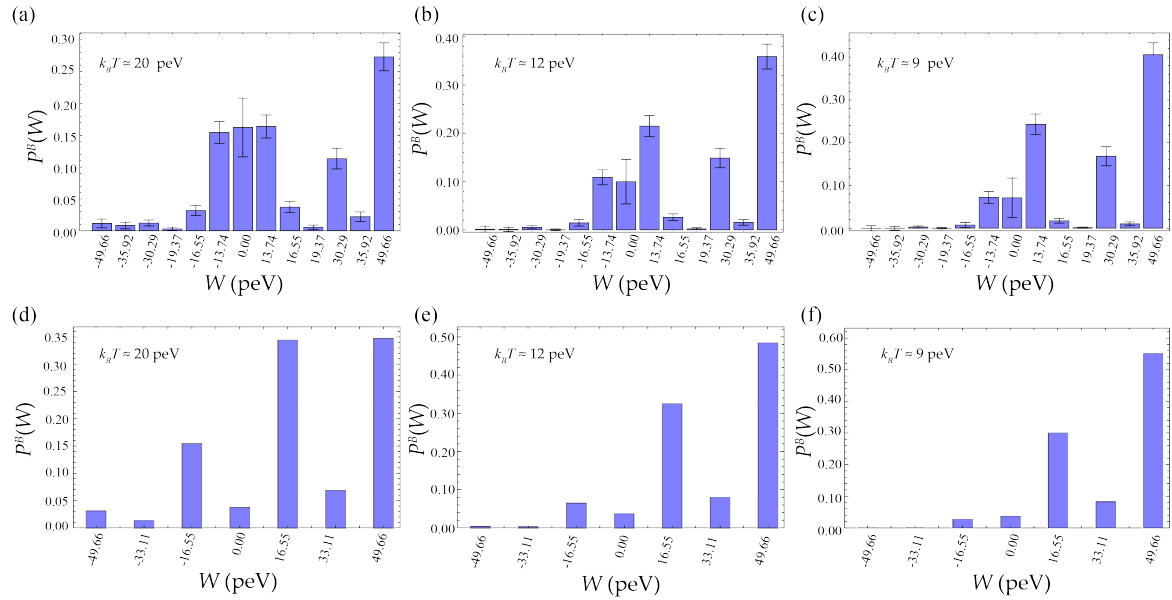

Figure S5. Experimental (a, b, c) and non-interacting theoretical (d, e, f) results for the backward work distribution for the three different initial spin temperatures (a, d) $k_BT = 20 \pm 3$ peV, (b, e) $k_BT = 12 \pm 2$ peV and (c, f) $k_BT = 9 \pm 2$ peV.